Discrimination of myelofibrosis and liver cirrhosis using a spleen ultrasound-based radiomics nomogram model

SI-CHEN CHEN[1*], YAN DING[1*], XIN-YI XU[1] and SHU-YING ZHANG[2]

[1]Department of Ultrasound Medicine, The Affiliated Wuxi People's Hospital of Nanjing Medical University, Wuxi, Jiangsu 214023, P.R. China; [2]Department of Ultrasound, The Second Affiliated Hospital of Soochow University, Suzhou, Jiangsu 215004, P.R. China

Received May 20, 2025; Accepted September 4, 2025

DOI: 10.3892/etm.2025.12981

Abstract. The aim of the present study was to develop and validate a spleen ultrasound-based radiomics nomogram for non-invasive differentiation between myelofibrosis (MF) and liver cirrhosis. A total of 90 patients (40 patients with MF and 50 with cirrhosis) were enrolled, and randomly divided into training (n=72) and validation (n=18) sets. Ultrasound radiomics features were extracted from spleen images using PyRadiomics, and feature selection was performed using the least absolute shrinkage and selection operator and Boruta algorithms. Multivariate logistic regression combining radiomics features and clinical parameters was used to construct the nomogram model. Two radiomics features (wavelet.HHL_glcm_ClusterShade and original_glszm_GrayLevelNonUniformity) were selected. When combined with direct bilirubin and glutamic-oxalacetic transaminase levels, the nomogram achieved an area under the curve of 0.958 [95% confidence interval (CI), 0.912-1.0] in the training set and 0.750 (95% CI, 0.487-1.0) in the validation set, with sensitivities of 93.8 and 100%, specificities of 87.5 and 60%, and accuracies of 80.3 and 71.4%, respectively. In conclusion, the spleen ultrasound-based radiomics nomogram demonstrated promising performance for differentiating MF from liver cirrhosis, providing a potential non-invasive tool for early diagnosis and clinical decision-making.

Introduction

The spleen is the largest lymphoid organ in the body, and plays a pivotal role in regulating hematologic and immune homeostasis (1). A wide range of conditions, including hematologic malignancies, infections and inflammatory disorders (systemic lupus erythematosus, rheumatoid arthritis, sarcoidosis), can induce alterations in splenic volume, morphology and metabolic activity (2). Imaging serves as a critical tool for evaluating splenic architecture, facilitating the distinction between focal and diffuse patterns of involvement (3). Among these, diffuse infiltration poses the greatest diagnostic challenge, arising from either the accumulation of normal or neoplastic cellular elements, or from congestion due to hyperemia and impaired venous outflow (3).

Myelofibrosis (MF) is a myeloproliferative neoplasm of unclear etiology. MF is a rare disorder that typically progresses insidiously during the early-stage and is characterized by non-specific clinical manifestations (fatigue, weight loss, night sweats, and mild abdominal discomfort), contributing to a high rate of misdiagnosis (4). Early-stage MF often presents with splenomegaly and cytopenia, clinical features that can be readily mistaken for liver cirrhosis (5,6). Consequently, patients frequently first seek medical evaluation in gastroenterology or infectious disease clinics, reflecting the subtlety of hematologic abnormalities at presentation. Due to the limited familiarity with MF within these clinics, treatment is often suboptimal. MF has frequently advanced to the intermediate or late stages before patients are referred to the hematology department, which results in poor treatment outcomes and prognosis (7). Hence, there is a critical need for early differential diagnosis between MF and liver cirrhosis. Non-invasive methods are particularly valuable for assessing the underlying causes of splenic involvement in patients, given the constraints of splenic biopsy. Distinguishing variations based on the qualitative features of spleen cross-sectional images is a notable challenge (8).

Radiomics, an emerging tool in precision medicine, leverages advanced algorithms to automatically extract quantitative features, such as lesion intensity, morphology and texture, from medical imaging datasets. These features can then be integrated into predictive models that enhance clinical decision-making (9). To the best of our knowledge, no studies have directly compared ultrasound-based radiomic signatures of splenomegaly attributable to MF vs. liver cirrhosis. The present study aimed to develop a nomogram incorporating clinical and ultrasound radiomics features of the spleen to noninvasively distinguish early-stage MF from cirrhosis, thereby offering a valuable reference for guiding therapeutic strategies and patient management.

Correspondence to: Dr Shu-Ying Zhang, Department of Ultrasound, The Second Affiliated Hospital of Soochow University, 1055 Sanxiang Road, Suzhou, Jiangsu 215004, P.R. China
E-mail: shuyingzhang506@hotmail.com

*Contributed equally

Key words: spleen, radiomics, myelofibrosis, liver cirrhosis

Materials and methods

Study cohort. The present retrospective study included a total of 40 patients with confirmed MF and treated at Wuxi People's Hospital (Wuxi, China) or The Second Affiliated Hospital of Soochow University (Suzhou, China) between January 2020 and August 2024 were included in the present study. The MF cohort comprised of 22 male patients and 18 female patients, aged between 53 and 73 years, with an average age of 62.93±12.96 years (mean ± SD). Additionally, 50 patients with clinically diagnosed hepatitis B-related cirrhosis and portal hypertension were selected from the same institutions during the same period. The cirrhosis group included 36 male and 14 women, aged between 40 and 75 years, with an average age of 50.93±12.96 years. The patients were randomly allocated into a training set consisting of 72 cases (including 32 patients with MF) and a validation set comprising of 18 cases (including 8 patients with MF). Allocation was performed using stratified sampling at an 8:2 ratio. The inclusion criteria comprised: i) Availability of complete, unannotated ultrasound images suitable for analysis; ii) a definitive clinical diagnosis supported by comprehensive clinical data and the absence of prior surgical intervention; and iii) no history of treatment prior to imaging. The exclusion criteria encompassed: i) Normal splenic volume; ii) splenic infarction; iii) presence of cystic or solid splenic lesions; and iv) thrombosis of the portal or splenic veins. The present study was approved by The Medical Ethics Committee of Wuxi People's Hospital (approval no. KY23017). Written informed consent was obtained from the patients for participation and for the publication of clinical details and accompanying images.

Clinical data collection. The electronic medical record system was used to retrieve the clinical data of patients, including the direct bilirubin level, glutamic-pyruvic transaminase, γ-glutamyl transferase, glutamic-oxalacetic transaminase and the isozyme of glutamic-oxalacetic transaminase, as well as complete blood count parameters including platelet counts.

Ultrasound examination. All ultrasound examinations were performed using standardized settings: Frequency 3.5-5 MHz, dynamic range 60-65 dB, gain 50-60%, depth 15-20 cm, focus position at the level of the spleen, and tissue harmonic imaging enabled. Images were saved in DICOM format with a resolution of 1,024x768 pixels without compression. All examinations were performed by sonographers with >5 years of experience in abdominal imaging. All patients were required to fast for 8 h before the examination. The present study utilized the LOGIQ™ E9 color Doppler ultrasound diagnostic instrument (GE Healthcare) equipped with a convex array probe operating at 3.5-5 MHz. Patients were positioned in a supine stance, with their left arm raised above their head to optimize the supracostal access. The probe was placed between the 9th and 11th left ribs to capture the oblique section of the major axis of the spleen. The maximum major-axis section of the spleen was preserved for subsequent analysis. The major axis and thickness of the spleen were recorded by identifying the section with the maximum major axis, with three measurements averaged for accuracy. Portal vein diameter was measured at the crossing point of the hepatic artery and splenic vein diameter was measured 2 cm from the splenic hilum during quiet respiration. These measurements were averaged from three consecutive readings during the same examination for accuracy. These procedures were documented and assessed by two ultrasonography physicians, each with >10 years of diagnostic experience. The physicians were blinded to each other's diagnoses and pathological findings. Any discrepancies in diagnoses were resolved through discussion to reach a consensus.

Image segmentation and data preprocessing. A high-resolution image of the maximum major-axis section of the spleen was imported into 3D-Slicer version 5.4 (slicer.org) in JPG format. Two experienced ultrasonography physicians, each with >10 years of diagnostic expertise, drew boundaries around the edge of the spleen on the image. This ensured that the entire spleen was encompassed within the largest possible region of interest (ROI). In cases where the discrepancy between the two ROIs drawn by the physicians (calculated as the ratio of the combined area of non-overlapping parts to the total area of both ROIs) was <5%, the ROI was defined as the overlapping region of the two. If the discrepancy was >5%, the physicians discussed this and reached a consensus. Fig. 1 illustrates the ROI delineation process, showing the original grayscale ultrasound image of an enlarged spleen (Fig. 1A) and the same image with manual ROI segmentation performed by experienced sonographers (Fig. 1B).

To assess segmentation reproducibility, 30 randomly selected cases (33%) were independently re-segmented (ROI redrawn) by both ultrasonography physicians after a 4-week interval to minimize recall bias. The inter-observer intra-class correlation coefficient (ICC) for ROI segmentation was 0.892 [95% confidence interval (CI), 0.845-0.932], and the intra-observer ICCs were 0.916 (95% CI, 0.878-0.948) for observer 1 and 0.909 (95% CI, 0.869-0.943) for observer 2. For radiomics feature extraction, an inter-observer ICC of >0.85 for 782/837 features (93.4%) and intra-observer ICC of >0.90 for 801/837 features (95.7%) was achieved. Only features with an ICC of >0.75 were retained for subsequent analysis.

Feature selection of ultrasound radiomics. The PyRadiomics module in Python version 3.9 (Python Software Foundation) was used to extract radiomics features from the grayscale ultrasound images. Initially, the ICC was utilized to assess the consistency of feature extraction between and within observers in the ROI. Higher ICC indicated greater consistency and improved repeatability. The analysis moved forward to the feature screening stage when the ICC was >0.75 in both groups. A total of 837 radiomics features were extracted, and Z-score normalization was applied to standardize these features and mitigate the effects of varying dimensions. Subsequently, two dimensionality reduction methods were employed to refine the selection from the 837 features, which ensured a more manageable set for analysis: i) The least absolute shrinkage and selection operator (LASSO) algorithm, with 5-fold cross-validation, was implemented to compress certain regression coefficients. This was achieved by introducing a penalty function that reduced the sum of the coefficients' absolute values below a predetermined threshold. The glmnet package (version 4.1-7) in R software (version 4.3.3, R Foundation for Statistical Computing), with family=binomial for binary result data. Key parameter α was set to 1 and cross-validation was

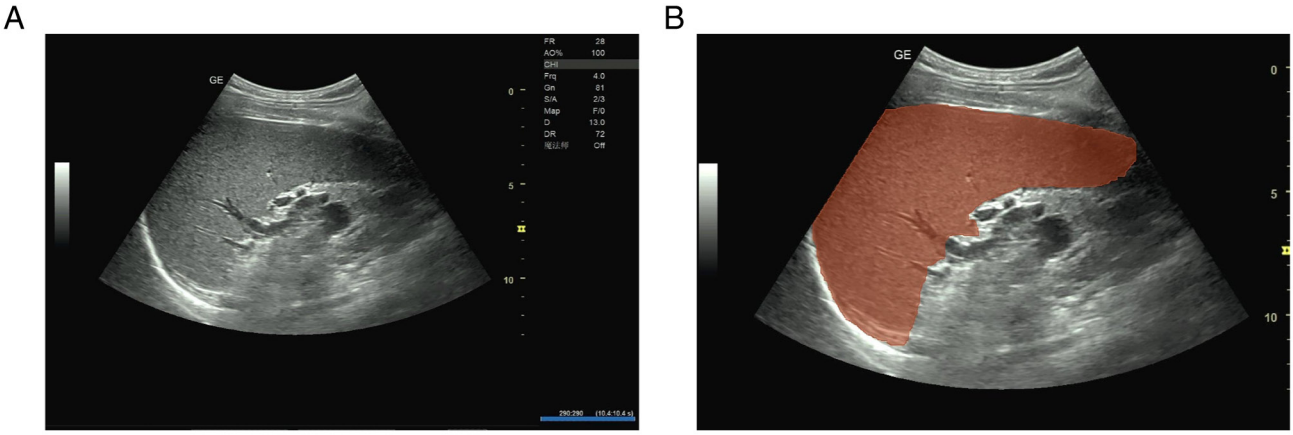

Figure 1. ROI target volume delineation on spleen ultrasound images. (A) Original grayscale ultrasound image showing the maximum long-axis section of an enlarged spleen in a patient with myelofibrosis. The spleen boundaries are clearly visible with homogeneous echotexture. (B) The same image with manual ROI delineation (orange overlay) performed by an experienced sonographer, encompassing the entire splenic parenchyma while carefully excluding surrounding structures. The ROI covers 95% of the visible spleen area, avoiding edge artifacts and adjacent organs. Scale bar, 5 cm. ROI, region of interest.

conducted using the cv.glmnet function. Two λ values, λ.min and λ.1se, were chosen: λ.min minimized cross-validation errors, while lambda.1se favored a more succinct model. The two provided a balance between model complexity and prediction accuracy. Ultimately, variables significant to prediction were identified based on non-zero coefficients, which simplified the model and enhanced interpretability. ii) The Boruta algorithm, a feature selection technique rooted in a random forest, assessed feature importance by creating shadow variables for each original variable in the dataset. Utilizing Boruta package version 8.0.0 (cran.r-project.org/package=Boruta) for feature selection, the algorithm systematically compared the significance of each original variable against its shadow counterpart. The importance of each variable was confirmed after 500 iterations or when all variables showed stability. The final results were extracted using the attStats function in R, and the format was refined with a custom adjustdata function in R

Establishment of a joint clinical-radiomics model. Independent predictors for differentiating liver cirrhosis from MF were identified using multivariate logistic regression. Analysis was based on the independent influencing factors of selected clinical and ultrasound characteristics, along with ultrasound radiomics features from the training set. Subsequently, a comprehensive clinical-radiomics model was developed and a corresponding nomogram was created.

Statistical processing. Data analysis was conducted using R (version 4.3.3), Python (version 3.7), and SPSS 27.0 (IBM Corp.) statistical software. Measurement data that adhered to a normal distribution are presented as the mean ± SD, with independent sample t-tests performed for group comparisons. Categorical data are presented as case counts, and χ^2 test was used for group comparisons. No categorical variables met criteria for statistical analysis in this cohort. The predictive efficacy of the model in the training and validation sets was evaluated by creating receiver operating characteristic curves and determining the area under the curve (AUC). P<0.05 (two-tailed) was considered to indicate a statistically significant difference.

Results

Selection of ultrasound radiomics feature. Using the PyRadiomics software package, 837 ultrasound image features of the spleen were extracted. Two key radiomics features were identified after dimensionality reduction by LASSO and Boruta algorithms: wavelet.HHL_glcm_ClusterShade (C1) and original_glszm_GrayLevelNonUniformity (C2) (Fig. 2).

Univariate and multivariate analyses of clinical and ultrasound radiomics data. The training set consisted of 72 patients, including 40 patients diagnosed with liver cirrhosis and 32 patients with MF. In univariate analysis, significant differences in C2, direct bilirubin, glutamic-pyruvic transaminase, glutamic-oxalacetic transaminase and the major axis of the spleen were observed between the two groups (all P<0.05). However, the C1, thickness of the spleen, γ-glutamyl transferase and glutamic-oxalacetic transaminase isozymes had no statistical significance between the two groups (all P>0.05; Table I).

As show in Table I, univariate analysis revealed significant differences in portal vein diameter between the two groups, with the liver cirrhosis group showing larger portal vein diameters compared with the MF group (13.6±1.55 vs. 12.4±1.31 mm, P=0.002). However, splenic vein diameters showed no statistically significant difference between the groups (9.5±1.5 vs. 9.6±2.2 mm, P=0.826). In the multivariate logistic regression analysis (Table II), portal vein diameter did not emerge as an independent predictor for differentiating the two conditions. Platelet count showed significant differences between the two groups (Table I: 96.00±19.60 vs. 155.50±114.00 x10^9/l, P=0.033), with both conditions demonstrating thrombocytopenia but to varying degrees. The MF group showed more variable platelet counts (ranging from 54-488 x10^9/l) compared with the liver cirrhosis group.

The dependent variable was coded as liver cirrhosis=0 and MF=1. Multivariate logistic regression analysis included all variables with P<0.05 in univariate analysis: C2, direct bilirubin, glutamic-pyruvic transaminase, glutamic-oxalacetic transaminase, and the major axis of the spleen. Forward

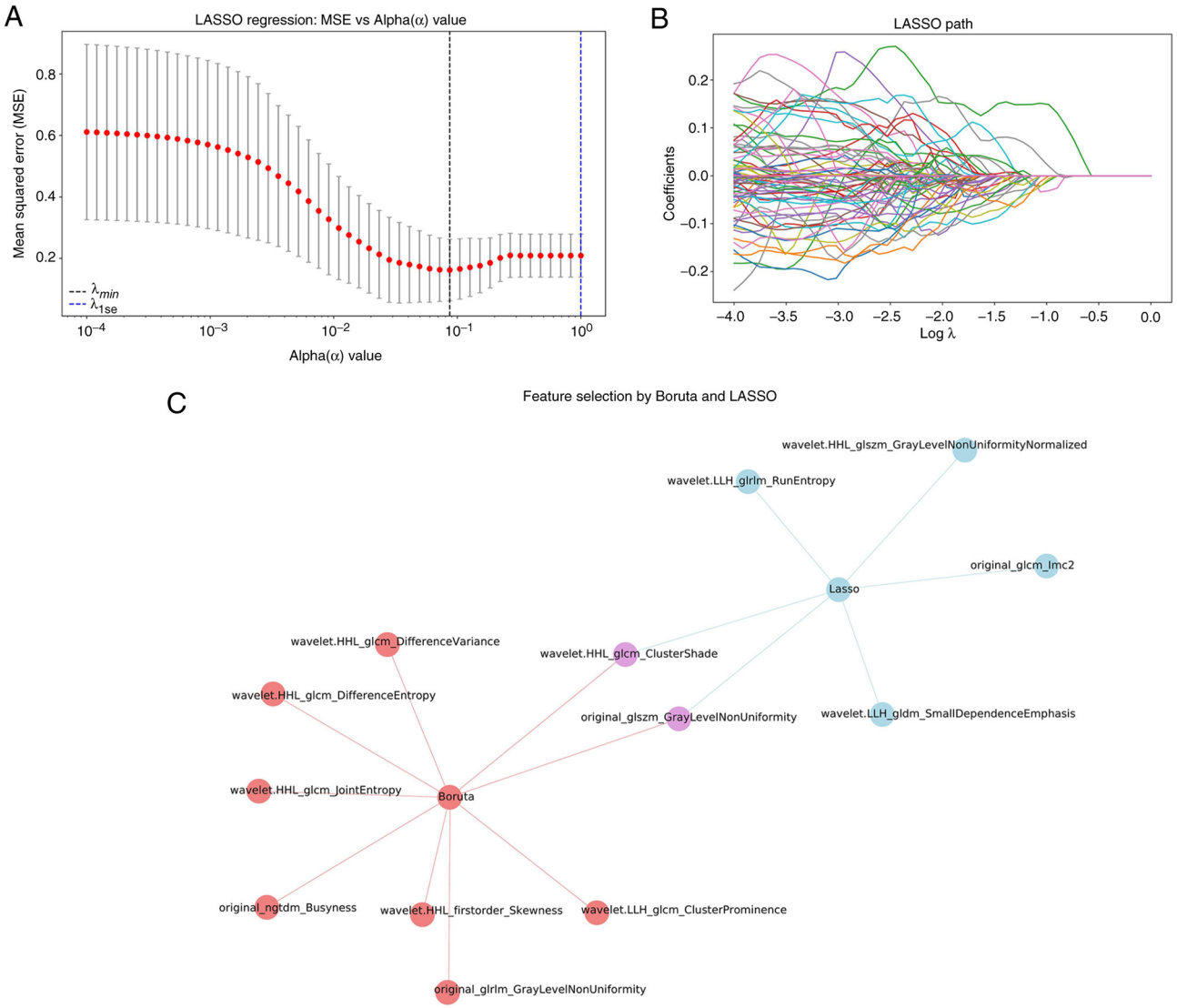

Figure 2. Selection of ultrasound radiomics features. (A) Feature selection of MSE and α value in LASSO regression. (B) LASSO path. (C) Screen of optimal parameters by LASSO and Boruta algorithms. LASSO, least absolute shrinkage and selection operator; MSE, mean squared error.

stepwise selection retained three variables in the final model. C2, direct bilirubin and glutamic-oxalacetic transaminase were identified as independent predictors for differentiating liver cirrhosis from MF. The logistic regression equation for predicting MF probability is: Logit (P)=2.895 + 3.694 x C2 -0.376x direct bilirubin -0.211 x glutamic-oxalacetic transaminase, where P represents the probability of MF diagnosis (Table II).

Model construction and predictive diagnosis effectiveness. A nomogram model was developed by incorporating two radiomics features (C1 and C2) and two clinical parameters (direct bilirubin and glutamic-oxalacetic transaminase levels) (Fig. 3). The model showed an AUC of 0.958 (95% CI, 0.912-1.0) for the training set and 0.750 (95% CI, 0.487-1.0) for the validation set (Fig. 4A and B). The model also achieved 93.8% sensitivity, 87.5% specificity and 80.3% accuracy for the training set, and 100% sensitivity, 60% specificity and 71.4% accuracy for the validation set. The concordance between liver cirrhosis and clinical diagnosis was 70% (35/50), and it was 100% (40/40) for MF. Fig. 4C-E presents the calibration and decision curves for both the training and validation sets.

Model validation and stability analysis. To assess potential overfitting given the difference between training (AUC=0.958) and validation (AUC=0.750) performance, additional validation analyses were performed. Five-fold cross-validation within the training set yielded a mean AUC of 0.856 (95% CI, 0.792-0.920), suggesting more modest performance than the initial training AUC. Bootstrapping with 1,000 iterations revealed confidence intervals of 0.889-0.987 for the training AUC, confirming model stability. When a more stringent feature selection was applied using λ.1se instead of λ.min, the model retained only the two most robust features (C2 and C1), supporting their importance for differentiation.

Discussion

The spleen, a central lymphoid organ, plays a critical role in the pathophysiology of infections (infectious mononucleosis,

Table I. Univariate analysis of clinical and ultrasound radiomics data in the training set.

Variable	Liver cirrhosis	Myelofibrosis	t-value	P-value
C1	0.01±0.87	0.63±1.11	2.054	0.051
C2	0.70±0.28	1.30±0.60	-3.790	0.001
Spleen major ais (mm)	151.00±25.80	170.00±20.70	-2.883	0.007
Spleen thickness, (mm)	56.2±12.60	66.70±6.60	-1.746	0.087
Direct bilirubin (μmol/l)	18.00± 6.60	6.30±4.30	2.679	0.010
Glutamic-pyruvic transaminase (U/l)	38.00±30.90	18.50±9.40	3.586	<0.001
γ-glutamyl transferase (U/l)	69.40±105.00	37.90± 3.40	1.789	0.079
Glutamic-oxalacetic transaminase (U/l)	55.70±45.90	21.40±4.10	4.676	<0.001
Glutamic-oxalacetic transaminase isozyme (U/l)	16.70±8.60	12.90±5.90	1.874	0.068
Platelet count (x10^9/l)	96.00±19.60	155.50±114.00	-2.292	0.033
Portal vein (mm)	13.60±1.55	12.40±1.31	3.361	0.002
Splenic vein (mm)	9.50±1.50	9.60±2.20	-0.221	0.826

Data are presented as mean ± standard deviation. C1 and C2 are standardized radiomics features (dimensionless). Independent samples t-test was used for all comparisons.

Table II. Multivariate analysis of clinical and ultrasound radiomics data in the training set.

Variable	Regression coefficient	Standard error	Wald χ^2 value	P-value	OR value (95% confidence intervals)
C2	3.694	1.608	5.279	0.022	40.218 (1.721-940.008)
Direct bilirubin	-0.376	0.166	5.146	0.023	0.687 (0.496-0.950)
Glutamic-oxalacetic transaminase	-0.211	0.104	4.137	0.042	0.810 (0.660-0.992)
Constant	2.895	2.319	1.559	0.212	18.092 (-1.653 - 7.443)

OR, odds ratio.

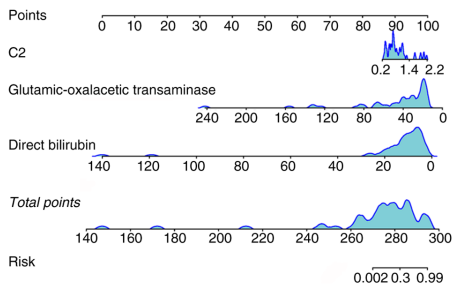

Figure 3. Clinical-radiomics nomogram for differentiating MF from liver cirrhosis. To use this nomogram, the following instructions should be followed: i) Locate the patient's C2 value on the 'C2' axis and draw a vertical line to the 'Points' axis to determine the points for this variable; ii) repeat for glutamic-oxalacetic transaminase and direct bilirubin values; iii) sum all points and locate this value on the 'Total points' axis; iv) draw a vertical line down to the 'Risk' axis to determine the probability of MF. For example, a patient with C2=1.5, glutamic-oxalacetic transaminase=30 U/l and direct bilirubin=10 μmol/l would have ~75% probability of MF rather than liver cirrhosis. MF, myelofibrosis.

malaria), metabolic disorders (e.g., Gaucher and Niemann-Pick disease), and hematologic diseases (e.g., lymphoma, leukemia) (10-12). Splenomegaly, defined as enlargement of the spleen, is a frequent clinical manifestation and underlying etiology is pivotal for guiding targeted therapy (13). In MF extramedullary hematopoiesis within the liver and spleen contributes to secondary portal hypertension, characterized by increased splenic blood flow and elevated resistance within hepatic sinusoids, ultimately leading to splenomegaly. In ~50% of patients with MF, the presented symptoms are attributable to portal hypertension at initial diagnosis (14). Among these, gastrointestinal hemorrhage is the most prevalent, followed by other complications of portal hypertension, such as ascites, fatigue and abdominal distension,- clinical features that often lead to misdiagnosis as liver cirrhosis.

Researchers have highlighted the difficulty in differentiating splenomegaly due to early-stage MF or liver cirrhosis (15,16). Thus, a reliable and non-invasive diagnostic method is essential for clinical management. Ultrasound is the preferred imaging technique for spleen examination: Ultrasound radiomics involves extracting numerous quantitative parameters from ultrasound images that are indiscernible to the human eye. The parameter features reflect the internal differences in biological information of the lesion; therefore, these parameters can aid in precise diagnosis, differentiation, risk stratification and treatment evaluation. Consequently, the

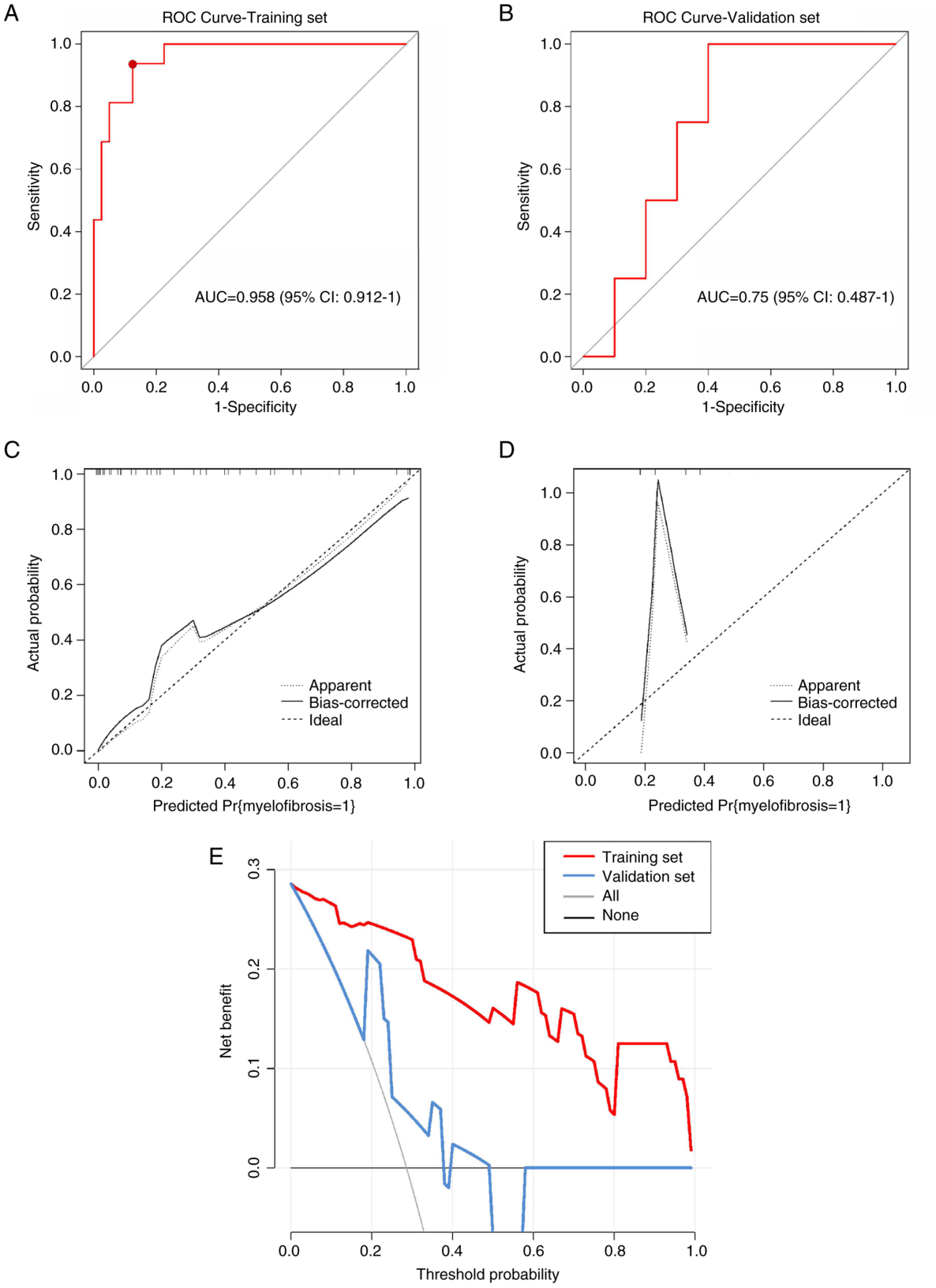

Figure 4. Model performance validation and clinical utility assessment. (A) ROC) curve for the training set (n=72). The curve demonstrates excellent discrimination with AUC=0.958 (95% CI, 0.912-1.0). The optimal cutoff point (sensitivity=93.8%, specificity=87.5%) is marked with a red dot. (B) ROC curve for the validation set (n=18). The curve shows moderate discrimination with AUC=0.750 (95% CI, 0.487-1.0), indicating acceptable but reduced performance compared to the training set. (C) Calibration curve for the training set. The plot demonstrates excellent agreement between predicted probabilities (x-axis) and observed frequencies (y-axis), with the calibration line closely following the diagonal reference line (perfect calibration). (D) Calibration curve for the validation set. The plot shows moderate calibration with some deviation from the diagonal reference line, particularly at higher predicted probabilities, suggesting slight model overconfidence in this cohort. (E) Decision curve analysis for clinical utility assessment. The graph displays net benefit (y-axis) across threshold probabilities (x-axis, 0-1.0). The nomogram model (red line) provides superior clinical utility compared to treat-all strategy (blue line) or treat-none strategy (black horizontal line at net benefit=0) for threshold probabilities between 0.1 and 0.8. ROC, receiver operating characteristic; AUC, area under the curve; CI, confidence interval.

present study utilized ultrasound radiomics to extract considerable microscopic information from spleen ultrasound images in patients with MF or liver cirrhosis; combining ultrasound radiomics with high-risk clinical factors, a nomogram model was developed to differentiate MF from liver cirrhosis.

The present study sought to develop a comprehensive model integrating clinical and ultrasound radiomics data to enhance the differentiation between MF and liver cirrhosis. Clinically, significant disparities were noted in direct bilirubin, glutamic-pyruvic transaminase and glutamic-oxalacetic transaminase levels between the two conditions. Xie *et al* (17) previously concluded that differences in glutamic-pyruvic transaminase, lactate dehydrogenase and direct bilirubin across MF and liver cirrhosis groups have statistical significance, which is consistent with the findings of the present study. Patients with MF retain normal liver cell function; thus, their synthetic, transformative and metabolic abilities are unaffected. By contrast, patients with liver cirrhosis suffer from abnormal liver function due to the damage of liver cells. The platelet count differences observed in the present study reflect the distinct pathophysiological mechanisms of thrombocytopenia in these conditions. In liver cirrhosis, thrombocytopenia primarily results from splenic sequestration due to portal hypertension and reduced hepatic thrombopoietin production (18). By contrast, patients with MF exhibited more variable platelet counts, which is characteristic of the heterogeneous nature of the disease, some patients may present with thrombocytosis in early stages while others develop thrombocytopenia as bone marrow fibrosis progresses (19). This variability in platelet counts in patients with MF, compared with the more consistent moderate thrombocytopenia in cirrhosis, may serve as an additional diagnostic marker when integrated with other clinical and imaging findings in individual patient assessment. However, platelet count alone was not retained as an independent predictor in the multivariate model used in the present study, suggesting that the combination of radiomics features and liver function tests provides superior discriminative power.

Patients with liver cirrhosis maintain a constant liver size or experience a compensatory increase in size in the early stages, and it is only in the advanced stages that the liver begins to shrink (20). Spleen enlargement in early cirrhosis is typically moderate (13-15 cm) compared with marked splenomegaly (>20 cm) often seen in advanced MF. In addition, patients with MF often initially show no substantial blood system abnormalities (anemia, leukocytosis, or thrombocytosis) (21), with splenomegaly being the sole manifestation. As MF progresses, the enhanced extramedullary hematopoietic function leads to blockage of the hepatic veins, which in turn increases portal venous pressure and liver volume, and the spleen becomes moderately or more enlarged. The present study includes ultrasound image of the spleen of a patient with MF at the onset of the disease: In the case presented, the condition is mild and does not exhibit the typical features of severe spleen enlargement.

The findings of the present study regarding portal and splenic vein dimensions align with the pathophysiological differences between MF and liver cirrhosis. The significantly larger portal vein diameter in patients with liver cirrhosis reflects the well-established portal hypertension that characterizes this condition (22). By contrast, patients with MF showed relatively normal portal vein dimensions despite splenomegaly, suggesting that the splenic enlargement in MF is primarily due to extramedullary hematopoiesis rather than portal hypertension (23). Furthermore, splenic vein diameters were similar between groups in the present study, possibly due to compensatory mechanisms in both conditions. While these vascular parameters provide additional diagnostic insights, they did not independently predict disease type in the multivariate model presented in the current study, suggesting that the combination of radiomics features and liver function tests remains more discriminative.

Clinical vigilance is essential for cases presenting with anemia and splenomegaly but without hypohepatia, as these may indicate the presence of MF (24) It is recommended to conduct bone marrow aspiration and examination, and if necessary, a liver biopsy should be performed to investigate the presence of extramedullary hematopoiesis. MF) is a rare condition, with incidence rates reported between 0.1 and 1.9 cases/100,000 persons per year (25), and numerous patients do not receive an accurate clinical diagnosis until their death. Patients exhibiting early-stage splenomegaly in MF were included in the present study; however, some patients with MF who exhibited signs of greatly enlarged spleen had their condition misjudged during initial clinical evaluations, which delayed proper diagnosis, and consequently these patients were excluded due to incomplete imaging data from delayed referral. Therefore, the difference in splenic size between the two groups had no statistical significance in the multivariate logical regression analysis.

The present study pioneered the use of spleen radiomics for differentiating MF from liver cirrhosis. Spleen CT radiomics has been previously employed to distinguish lymphoma from benign splenomegaly (26); additionally, the characteristics of spleen CT radiomics have been utilized to forecast the prognosis of patients with esophageal squamous cell carcinoma (27). Furthermore, the relapse of hepatocellular carcinoma (HCC) has been predicted using the characteristics of CT spleen radiomics (28); these spleen-based radiomics models have demonstrated notable clinical predictive value. The clinical value of spleen radiomics is further demonstrated in the present study where the ultrasound radiomics approach, grounded in splenomegaly, enhanced the differentiation between MF and liver cirrhosis. The radiomics was able to convert medical imaging data into high-throughput data, encompassing features such as markings and shape characteristics that were not readily observable to the naked eye.

The pathophysiological mechanisms driving splenomegaly in MF and liver cirrhosis are fundamentally distinct. The spleen comprises two primary compartments: Red pulp and white pulp. The red pulp is composed of venous sinuses, reticular fibers, myofibroblasts and macrophages, whereas the white pulp contains the periarterial lymphatic sheath, follicles, and marginal zones enriched with lymphocytes, macrophages, dendritic cells and plasma cells. In liver cirrhosis, portal hypertension induces congestive splenomegaly predominantly involving the red pulp (29). Conversely, MF is characterized by infiltration of clonal hematopoietic cells into the white pulp and marginal zones. These divergent histopathological alterations manifest as distinct radiomics signatures on imaging (30).

The findings of the present study align with and extend previous radiomics applications in spleen imaging. Enke *et al* (26) used CT-based spleen radiomics to differentiate lymphoma from benign splenomegaly, achieving an AUC of 0.87, comparable to validation set performance in the present study. However, the previous study required radiation exposure, whereas in the present study the ultrasound-based approach offers a radiation-free alternative. Similarly, Li *et al* (28) demonstrated that spleen CT radiomics could predict HCC recurrence with an AUC of 0.82, suggesting that splenic texture changes reflect systemic disease states beyond primary splenic pathology.

The radiomics features identified in the present study (wavelet.HHL_glcm_ClusterShade and original_glszm_GrayLevelNonUniformity) reflect texture heterogeneity, consistent with texture heterogeneity findings in liver, kidney and pancreatic radiomics studies (31,32). These gray-level non-uniformity features have proven valuable in detecting tissue architectural disruption in pancreatic radiomics (AUC 0.85 for pancreatitis vs. normal) and renal radiomics (AUC 0.88 for chronic kidney disease staging), supporting their biological relevance across different pathological processes (33,34).

The ultrasound radiomics nomogram developed in the present study provides a non-invasive tool for differentiating MF from liver cirrhosis, addressing a critical diagnostic challenge in clinical practice. By combining readily available ultrasound imaging with routine laboratory tests, this approach could facilitate earlier referral to hematology specialists and reduce diagnostic delays that often result in suboptimal treatment outcomes. Therefore, this model has the potential to reduce the need for unnecessary bone marrow aspirations and pathological biopsies in some patients with liver cirrhosis. The validity and reliability of the ultrasound radiomics model were confirmed in the present study.

To facilitate clinical adoption of the nomogram model used in the present study, a three-tier implementation strategy should be implemented. First, for immediate implementation, a web-based calculator (accessible at frontiersin.org/articles/10.3389/fmed.2024.1474311/fulls) has been developed, where clinicians can input the two radiomics values (C2 and C1), direct bilirubin and glutamic-oxalacetic transaminase levels to obtain the probability of MF vs. liver cirrhosis. This requires only manual ROI drawing in existing Picture Archiving and Communication System (PACS) viewers and feature extraction using the provided script.

For medium-term integration (6-12 months), a PACS-integrated plugin that enables semi-automated workflow is currently in development, which will work as follows: i) The sonographer acquires standard spleen images and flags them for analysis; ii) a trained technician performs ROI segmentation using the standardized protocol presented in the current study (estimated time, 2-3 min); iii) radiomics features are automatically extracted and combined with laboratory values from the Electronic Medical Record system; and iv) the nomogram probability is calculated and displayed in the report template.

For long-term implementation, it is the aim to generate a fully automated system incorporating deep learning-based spleen segmentation. The preliminary testing shows that U-Net deep learning architecture can achieve Dice similarity coefficients of 0.89-0.92 based on preliminary validation using 50 test cases for spleen segmentation, reducing analysis time to <30 sec. However, this requires validation on larger datasets before clinical deployment.

The primary limitation of the present study is the relatively small sample size, particularly for patients with MF (n=40) and the validation cohort (n=18). This limitation reflects the rarity of MF, which has an incidence of only 0.5-1.5 per 100,000 person-years. Despite recruiting from two tertiary centers over 4.5 years, the strict inclusion criteria necessary for high-quality radiomics analysis (such as, standardized imaging protocols and the absence of prior treatment) further limited the cohort size. The substantial decrease in AUC from the training set (0.958) to the validation set (0.750) suggested potential overfitting despite the use of LASSO and Boruta algorithms for feature selection. To address these limitations and ensure model generalizability, a multicenter validation strategy should be conducted using the following criteria : i) Prospective enrollment from at least five hematology centers nationwide to achieve a target sample size of 200 patients with MF and 250 patients with liver cirrhosis over 3 years; ii) standardization of ultrasound acquisition protocols across centers with mandatory quality control measures; iii) implementation of external validation using completely independent datasets from different geographic regions; and iv) regular model recalibration every 6 months during the validation phase to maintain optimal performance. Discussions with the Chinese Hematology Ultrasound Consortium to implement this validation protocol will be initiated in the future.

In conclusion the model developed in the present study can distinguish patients with MF from those with liver cirrhosis in clinical settings, offering a valuable tool for early diagnosis and treatment. This advancement has the potential to markedly enhance patient care and outcomes. While the nomogram model shows promise for differentiating MF from liver cirrhosis, the current results should be interpreted with caution due to the limited sample size and evidence of overfitting. Larger, multicenter validation studies are essential before clinical implementation.

Acknowledgements

Not applicable.

Funding

The present study was funded by the Wuxi Double Hundred Program for Young and Middle-Aged Medical and Health Professionals (grant no. HB2023001).

Availability of data and materials

The data generated in the present study may be requested from the corresponding author.

Authors' contributions

SYZ designed the study, SCC and YD edited the manuscript. SCC and XYX collected data, processed the data and conducted the statistical analysis. YD and SYZ reviewed and

revised the manuscript. SYZ and YD confirm the authenticity of all the raw data. All authors read and approved the final manuscript.

Ethics approval and consent to participate

The present study was approved by the Medical Ethics Committee of Wuxi People's Hospital (approval no. KY23017). Written informed consent was obtained from participants for participation in the study and all methods were carried out in accordance with The Declaration of Helsinki.

Patient consent for publication

Written informed consent was obtained from the patients for the publication of clinical details and any accompanying images.

Competing interests

The authors declare that they have no competing interests.

References

1. Lewis SM, Williams A and Eisenbarth SC: Structure and function of the immune system in the spleen. Sci Immunol 4: eaau6085, 2019.
2. Garrison RN, McCoy M, Winkler C, Yam L and Fry DE: Splenectomy in hematologic malignancy. Am Surg 50: 428-432, 1984.
3. Reinert CP, Hinterleitner C, Fritz J, Nikolaou K and Horger M: Diagnosis of diffuse spleen involvement in haematological malignancies using a spleen-to-liver attenuation ratio on contrast-enhanced CT images. Eur Radiol 29: 450-457, 2019.
4. Dong HW, Hernandez L, Ghahremani JS, Chapek MA, Safran BA, Lau DL and Brewer MB: Venous stasis ulceration due to massive splenomegaly causing iliac vein compression from secondary myelofibrosis. Vasc Endovascular Surg 58: 769-772, 2024.
5. Klimova NF and Glasko EN: Myelofibrosis as one of the masks of liver cirrhosis. Gematol Transfuziol 28: 22-24, 1983 (In Russian).
6. Lu C, Hu XM, Bao WY, Zhou SY, Fan YQ, Ke J, Wang HS, Zhu RF, Liu Y, Fan L and Xiao SF: Primary biliary cirrhosis secondary to myelofibrosis: A case report and literature review. J Clin Hematol 31: 56-58, 2018.
7. Lee MW, Yeon SH, Ryu H, Song IC, Lee HJ, Yun HJ, Kim SY, Lee JE, Shin KS and Jo DY: Volumetric splenomegaly in patients with essential thrombocythemia and prefibrotic/early primary myelofibrosis. Int J Hematol 114: 35-43, 2021.
8. Gillies RJ, Kinahan PE and Hricak H: Radiomics: Images are more than pictures, they are data. Radiology 278: 563-77, 2016.
9. Liu Y, Li C, Guo J and Liu Y: A clinical-radiomics nomogram for differentiating focal organizing pneumonia and lung adenocarcinoma. Nan Fang Yi Ke Da Xue Xue Bao 44: 397-404, 2024 (In Chinese).
10. Breitfeld V and Lee RE: Pathology of the spleen in hematologic disease. Surg Clin North Am 55: 233-51, 1975.
11. Barthold D, Brouwer E, Barton LJ, Arterburn DE, Basu A, Courcoulas A, Crawford CL, Fedorka PN, Fischer H, Kim BB, *et al*: Minimum threshold of bariatric surgical weight loss for initial diabetes remission. Diabetes Care 45: 92-99, 2022.
12. Chang TC and Cavuoto KM: Binocular disturbance after glaucoma drainage device implantation. World J Ophthalmol 4: 25-28, 2014.
13. Wang X, He TT, Zhang N, Zhou C, Wang Q, Bai YF, Zhang JJ, Fu SG, Liang XX, Li X and Gong M: Clinical characteristics of 12 patients with primary myelofibrosis and liver cirrhosis. J Clin Hepatol 36: 2524-252, 2020.
14. Li R, Liu HS and Chen Y: Recent research advance to differentiate portal hypertension associated with primary myelofibrosis and cirrhosi. Chin J Exp Hematol 31: 598-601, 2023 (In Chinese).
15. Mazur R, Celmer M, Silicki J, Hołownia D, Pozowski P and Międzybrodzki K: Clinical applications of spleen ultrasound elastography-A review. J Ultrason 18: 37-41, 2018.
16. Webb M, Shibolet O, Halpern Z, Nagar M, Amariglio N, Levit S, Steinberg DM, Santo E and Salomon O: Assessment of liver and spleen stiffness in patients with myelofibrosis using fibroscan and shear wave elastography. Ultrasound Q 31: 166-9, 2015.
17. Xie QX, Jiang XP and Li X: Clinical characteristic analysis of 17 cases of primary myelofibrosis and portal hypertension. Chin J Infect Dis 31: 369-370, 2013.
18. Peck-Radosavljevic M: Thrombocytopenia in chronic liver disease. Liver Int 37: 778-793, 2017.
19. Yilmaz M and Verstovsek S: Managing patients with myelofibrosis and thrombocytopenia. Expert Rev Hematol 15: 233-241, 2022.
20. Ganeshan D, Bhosale P and Kundra V: Current update on cytogenetics, taxonomy, diagnosis, and management of adrenocortical carcinoma: What radiologists should know. AJR Am J Roentgenol 199: 1283-93, 2012.
21. Thiele J, Kvasnicka HM, Zankovich R and Diehl V: Early-stage idiopathic (primary) myelofibrosis-Current issues of diagnostic features. Leuk Lymphoma 43: 1035-1041, 2002.
22. Lafortune M, Marleau D, Breton G, Viallet A, Lavoie P and Huet PM: Portal venous system measurements in portal hypertension. Radiology 151: 27-30, 1984.
23. Johnson SS, Anslyn EV, Graham HV, Mahaffy PR and Ellington AD: Fingerprinting non-terran biosignatures. Astrobiology 18: 915-922, 2018.
24. Teodorescu P, Pasca S, Jurj A, Gafencu G, Joelsson JP, Selicean S, Moldovan C, Munteanu R, Onaciu A, Tigu AB, *et al*: Transforming growth factor β-mediated micromechanics modulates disease progression in primary myelofibrosis. J Cell Mol Med 24: 11100-11110, 2020.
25. Moulard O, Mehta J, Fryzek J, Olivares R, Iqbal U and Mesa RA: Epidemiology of myelofibrosis, essential thrombocythemia, and polycythemia vera in the European Union. Eur J Haematol 92: 289-97, 2014.
26. Enke JS, Moltz JH, D'Anastasi M, Kunz WG, Schmidt C, Maurus S, Mühlberg A, Katzmann A, Sühling M, Hahn H, *et al*: Radiomics features of the spleen as surrogates for CT-based lymphoma diagnosis and subtype differentiation. Cancers (Basel) 4: 713, 2022.
27. Guo L, Liu A, Geng X, Zhao Z, Nie Y, Wang L, Liu D, Li Y, Li Y, Li D, *et al*: The role of spleen radiomics model for predicting prognosis in esophageal squamous cell carcinoma patients receiving definitive radiotherapy. Thorac Cancer 15: 947-964, 2024.
28. Li P, Wu L, Li Z, Li J, Ye W, Shi Z, Xu Z, Zhu C, Ye H, Liu Z and Liang C: Spleen radiomics signature: A potential biomarker for prediction of early and late recurrences of hepatocellular carcinoma after resection. Front Oncol 11: 716849, 2021.
29. Bolognesi M, Merkel C, Sacerdoti D, Nava V and Gatta A: Role of spleen enlargement in cirrhosis with portal hypertension. Dig Liver Dis 34: 144-150, 2002.
30. Meng D, Wei Y, Feng X, Kang B, Wang X, Qi J, Zhao X and Zhu Q: CT-based radiomics score can accurately predict esophageal variceal rebleeding in cirrhotic patients. Front Med (Lausanne) 8: 745931, 2021.
31. Kraft WK and Waldman SA: Manufacturer's drug interaction and postmarketing adverse event data: What are appropriate uses? Drug Saf 24: 637-643, 2001.
32. Wang FY, Stankiewicz CA, Bennett NL and Myers JS: Hit the ground running: Engaging early-career medical educators in scholarly activity. Acad Med 94: 1837, 2019.
33. Matsumoto S, Imamura H, Takayanagi A, Fukumitsu R, Goto M, Sunohara T, Fukui N, Omura Y, Akiyama T, Fukuda T, *et al*: First-in-human trial of center wire for neuroendovascular therapy to avoid guidewire-related complications. Interv Neuroradiol 31: 532-538, 2025.
34. Zhao W, Bendickson L and Nilsen-Hamilton M: The lipocalin2 gene is regulated in mammary epithelial cells by NFκB and C/EBP in response to mycoplasma. Sci Rep 10: 7641, 2020.